The far side of Mars: two distant marsquakes detected by InSight - Supplementary Material

Anna C. Horleston, John F. Clinton, Savas Ceylan, Domenico Giardini, Constantinos Charalambous, Jessica C.E. Irving, Philippe Lognonné, Simon C. Stähler, Géraldine Zenhäusern, Nikolaj L. Dahmen, Cecilia Duran, Taichi Kawamura, Amir Khan, Doyeon Kim, Matthieu Plasman, Fabian Euchner, Caroline Beghein, Éric Beucler, Quancheng Huang, Martin Knapmeyer, Brigitte Knapmeyer-Endrun, Vedran Lekić, Jiaqi Li, Clément Perrin, Martin Schimmel, Nicholas C. Schmerr, Alexander E. Stott, Eléonore Stutzmann, Nicholas A. Teanby, Zongbo Xu, Mark Panning, William B. Banerdt

Supplemental Text

The marsquake service (MQS) uses a number of tools in their data analysis procedures. Here we present additional figures and information used by the MQS during analysis of these events.

Table 1 gives a comparative overview of the two distant marsquakes, S0976a and S1000a, detailing the location, phase picks and other pertinent information for each quake.

Figures S1 to S4 provide further information about event S0976a, whilst Table S2 lays out the glitches and donks (Scholz et al., 2020) which the MQS has noted in the data. In the same way, Figures S5 to S8 provide more information about S1000a and Table S3 indicates the approximate time of the glitches and donks noted for that event.

The filterbank images (Figures S1 and S5) show narrow-band energy envelopes for 20 sps VBB (very broadband) data. For S0976a, where the backazimuth is known, the filterbanks correspond to the vertical, radial and transverse components of the seismogram. For S1000a, where the backaziumth is unknown, the data are shown as vertical (Z), North (N) and East (E) components. This visualisation of the data allows the reader to see the frequency content and evolution of the waveforms across the duration of the events.

The comodulation plots (Figures S2 and S6) contain a spectrogram with the combined energy from all three (Z, N and E) components, and then combined power envelopes and pressure envelopes at a range of frequencies. For S1000a, pressure data was not available and the power around 4 Hz - a known lander resonance excited by wind - is use as a proxy for atmospheric injection. These images are used to understand the contributions of environmental signals to the seismic records (Charalambous et al., 2021). This is especially important with a surface-deployed sensor and allows for a more in depth analysis of the seismic energy.

The polarisation plots (Figures S3 and S7) are used to assess the direction and inclination of incoming energy. The polarisation analysis is based on the work of Samson and Olson (1980) and Samson (1983) and was further developed by Schimmel and Gallart (2003), Schimmel et al. (2011) and Stutzmann et al. (2021). This approach uses an eigen-analysis of the spectral matrix obtained after transforming the three-component seismic data in velocity into time-frequency domain using a continuous wavelet transform. A degree of polarisation filter (Samson, 1983) masks signals with weak polarisation to enhance the seismic signal.

Figures S4 and S8 offer alternatives to Figures 2 and 3 in the main text showing the full bandwidth of the data up to 100 Hz in panel (b) of each figure. There are many resonance modes (caused by vibrations of the lander (Dahmen et al., 2021)) and high-frequency glitches and donks (Scholz et al., 2020) that appear at higher frequencies but the majority of these are above the frequency range of interest for the two quakes. In figure S8(d) we also show the effect of low frequency glitches on the data. Although there are some prominent glitches and a tilt-induced drift within the time series, these artefacts do not interfere with the phase picks made by the MQS. We include these figures for completeness so that anyone studying the full data will understand some of the complexities of analysing the seismic data from InSight. Further details on the idiosyncrasies of the Martian seismic data set can be found in Ceylan et al. (2021) and Kim et al. (2021).

Event parameters	Event names S0976a	S1000a
Origin time		
UTC	2021-08-25 03:32:20	2021-09-18 17:48:00
LMST	02:20:20	00:48:25
Distance	146° (±7°)	116° (-9°, +31°)
Backazimuth	101° (±25°)	–
M_w^{Ma} ($M_{w,spec}^{Ma}$)	4.2 ± 0.3	4.1 ± 0.2
m_b^{Ma}	4.2	4.4
m_{bS}^{Ma}	4.4	4.6
Seismic Moment (N.m)	2.2×10^{15}	1.6×10^{15}
Peak amplitude (m/s)		
Vertical	5.2×10^{-9}	2.9×10^{-8}
North	8.1×10^{-9}	2.7×10^{-8}
East	8.8×10^{-9}	3.1×10^{-8}
Phase picks (UTC)		
Pdiff	–	17:59:01(±10 s)
PP	03:49:06(±10 s)	18:01:47(±20 s)
SS	04:03:07(±10 s)	18:14:08(±60 s)
y1	–	18:00:57(±5 s)
y2	–	18:14:08(±60 s)
Phase picks (relative to Origin time)		
Pdiff	–	661±10 s
PP	1006±10 s	827±20 s
SS	1847±10 s	1568±60 s
y1	–	777±5 s
y2	–	1568±60 s
SNR		
Seismic	33.1	1035.9
Pressure	33.8	–
Wind	–	–
Duration	~56 min	~94 min

Table S1: Summary of the event parameters and phase picks. The sol number for the LMST (Local Mean Solar Time) origin time is inferred from the event name. Seismic Moment is calculated following Kanamori (1977). MQS reports the signal-to-noise ratio (SNR) measurement from the seismic data, as well as pressure and wind data when available (Clinton et al., 2021). The wind sensors were not recording during both of the events. The pressure sensors were operational only during S0976a. Peak amplitude is picked on unfiltered rotated ZNE velocity data.

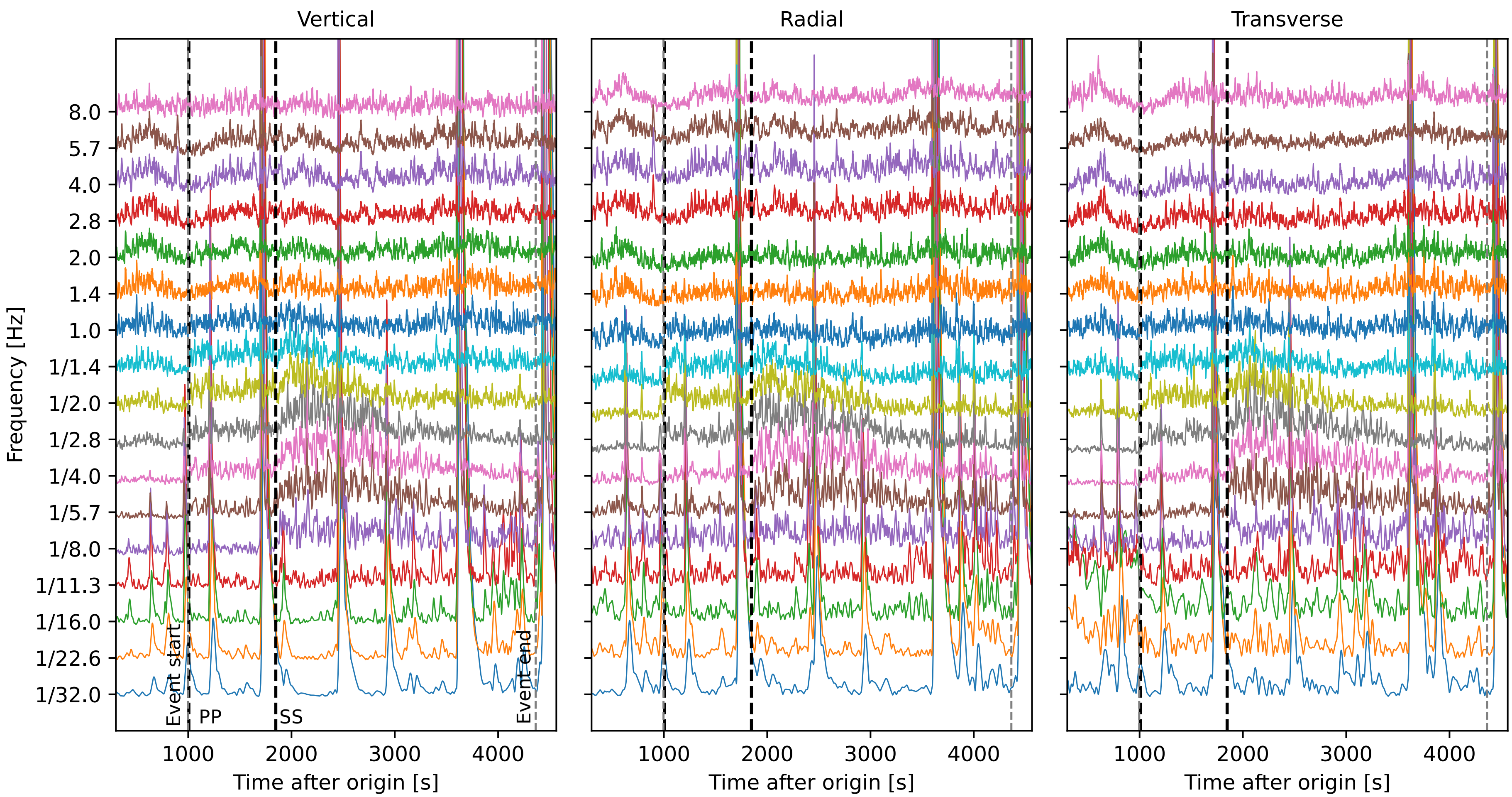

Figure S1: Filterbank for S0976a, using the 20 samples–per–second VBB (very broadband) data. The seismic components are rotated into vertical-radial-transverse framework, pointing towards the event's epicenter. The dashed vertical lines indicate V9 catalogue pick information: start and end times (grey) and phase picks (black). Each filtered trace has amplitude normalised by the 90th percentile amplitude of the whole trace. Glitches and donks show as high amplitude vertical spikes, broadening at lower frequencies. Note the relatively narrow banded PP arrival between 2 - 6 s and the broader, lower frequency SS arrival evident from 2 - 8 s period.

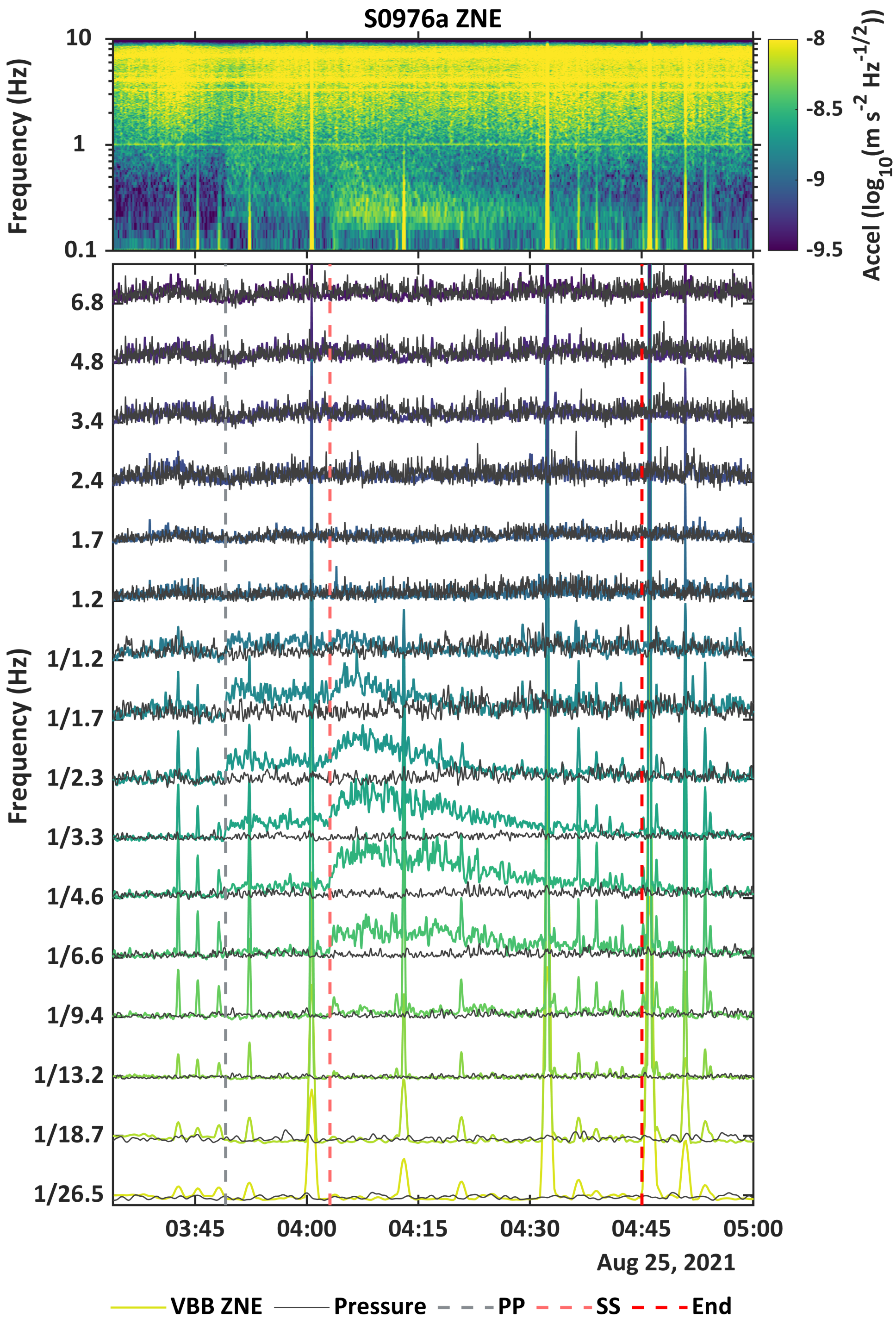

Figure S2: Comodulation for S0976a. Top panel: combined energy spectrogram for VBB (very broadband) ZNE. Lower panel: VBB ZNE power envelope and pressure envelope in different frequency bands. The PP and SS phases are marked by the grey and orange dashed lines respectively. The event end, as catalogued by MQS, is marked by the vertical red dashed line. Note the clear divergence of the seismic power from the pressure power from 1/2 Hz to 1/8 Hz and that the SS phase shows lower frequencies than the PP phase. It can be seen here that there is seismic energy in the PP phase below the 2 s that was evident in the filterbank. The SS phase shows an extended coda at lower frequencies.

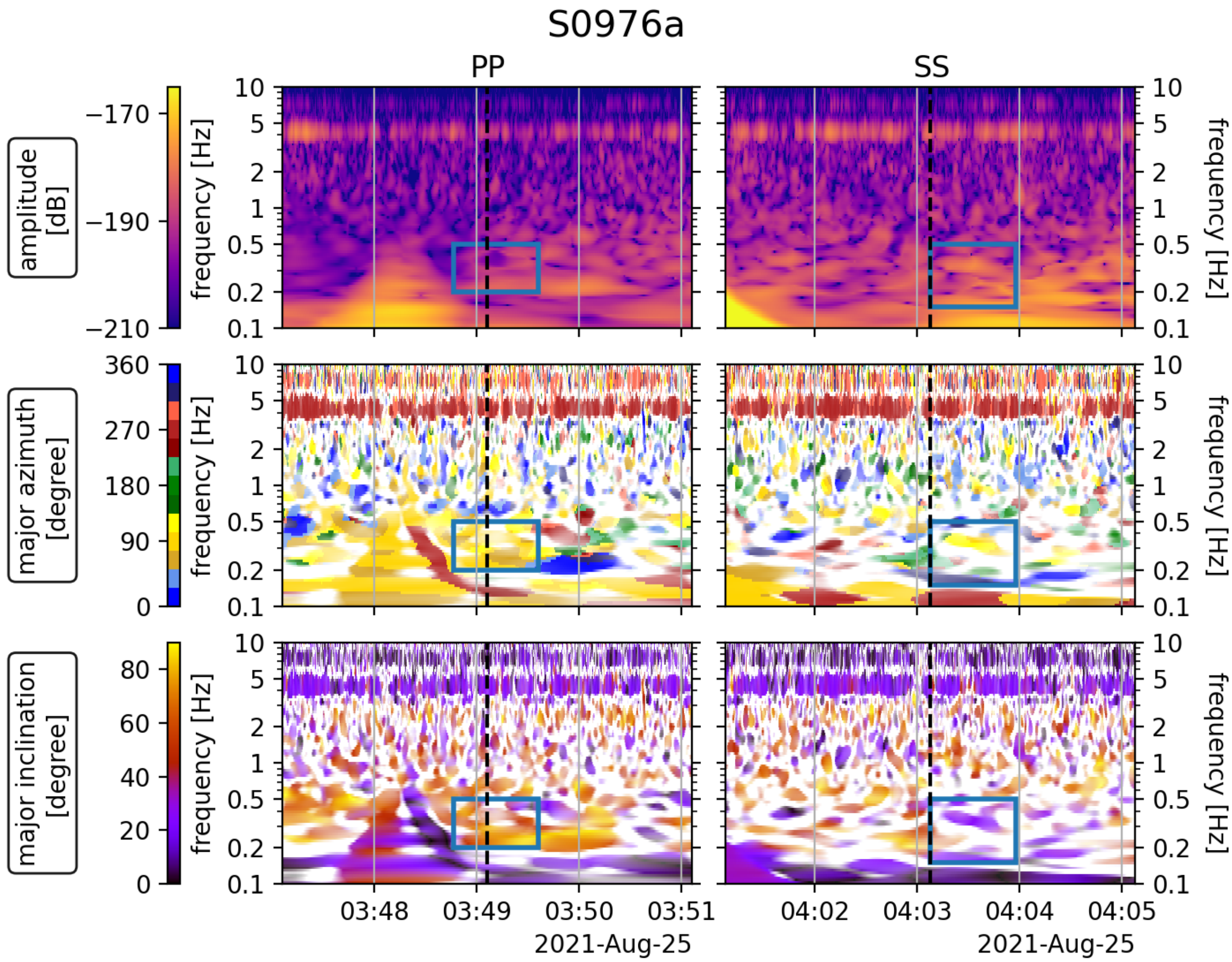

Figure S3: Polarisation analysis for marsquake S0967a. Shown are frequency-time plots of (top) signal amplitude in $(m/s)^2$/Hz [dB], (middle) backazimuth, and (bottom) inclination. The time axis is zoomed in on the (left) PP and (right) SS phase pick. Picks are marked with a vertical dashed line. Signals with weak polarisation are masked in the second and third row. Features to interpret are highlighted by blue boxes. The backazimuth was determined from the PP phase, supporting the particle motion analysis from the MQS GUI. The major inclination for each phase (towards vertical for PP and more horizontal for SS), highlighted in the third row supports the assignment of the phases as PP and SS.

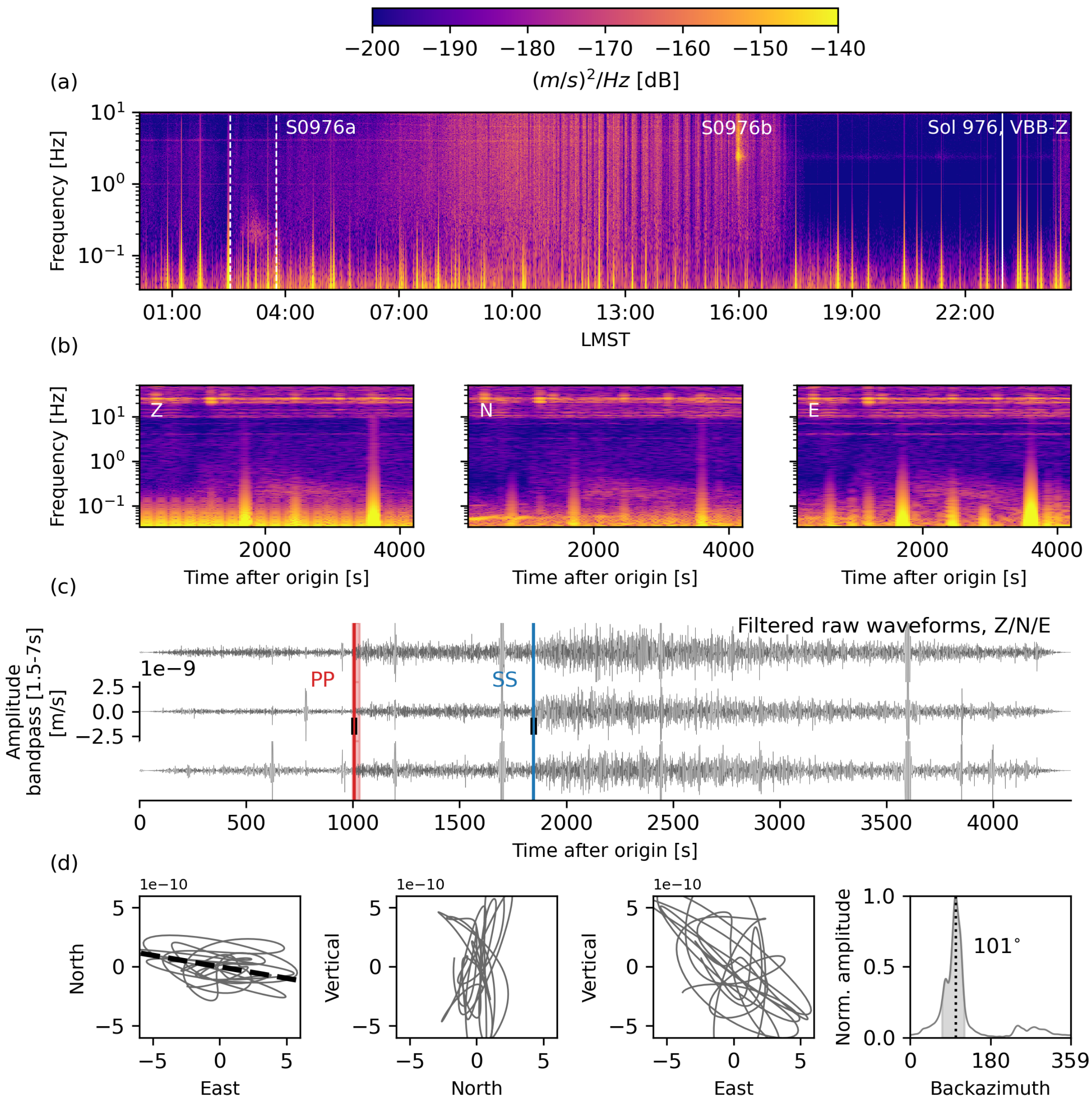

Figure S4: Overview of S0976a. (a) Sol-long velocity spectrogram for 20 sps (samples per second) VBB (very broadband) vertical component computed with a window length of 120 s and 50% overlap. The origin and signal end times are marked by vertical white dashed lines. A second event (S0976b, VF (very high frequency)) is also labelled. High-amplitude yellow transient spikes in all spectrograms are glitches or donks; the horizontal feature at 1 Hz (also referred to as *tick noise*) is an artefact from the Electronics Box measurement system (e.g. Ceylan et al., 2021). Other horizontal features during the windy periods are the lander modes at e.g., 4 Hz and the 2.4 Hz resonance, which is observed consistently during the quiet evening period. (b) velocity spectrograms for each VBB 100 sps component (Z, N, E; window length 200 s, 80% overlap) focused around the event as marked in (a). (c) VBB velocity waveforms filtered between 1.5–7 s. Vertical red and blue lines denote the PP and SS picks, respectively, with uncertainties marked by black error bars. The pink box around the PP pick indicates the time window used to create the hodograms in (d) for backazimuth determination. (d) also includes the backazimuth probability density function with 2σ errors marked in grey shade.

Table S2: Approximate onset times of glitches and donks during S0976a

Time (UTC)	Relative time (s)	Artefact type
2021-08-25 03:38:34	374	Donk
2021-08-25 03:42:42	622	Glitch
2021-08-25 03:45:20	780	Glitch
2021-08-25 03:48:10	950	Glitch
2021-08-25 03:48:21	961	Glitch
2021-08-25 03:52:17	1197	Glitch
2021-08-25 03:55:28	1388	Donk
2021-08-25 03:57:42	1522	Glitch
2021-08-25 04:00:39	1699	Glitch
2021-08-25 04:03:35	1875	Glitch
2021-08-25 04:03:58	1898	Glitch
2021-08-25 04:12:03	2383	Glitch
2021-08-25 04:13:02	2442	Glitch
2021-08-25 04:15:02	2562	Donk
2021-08-25 04:20:44	2904	Glitch
2021-08-25 04:23:21	3061	Glitch
2021-08-25 04:23:53	3093	Donk
2021-08-25 04:24:54	3154	Glitch
2021-08-25 04:32:09	3589	Donk
2021-08-25 04:32:19	3599	Glitch
2021-08-25 04:36:31	3851	Glitch
2021-08-25 04:38:57	3997	Glitch
2021-08-25 04:46:05	4425	Glitch

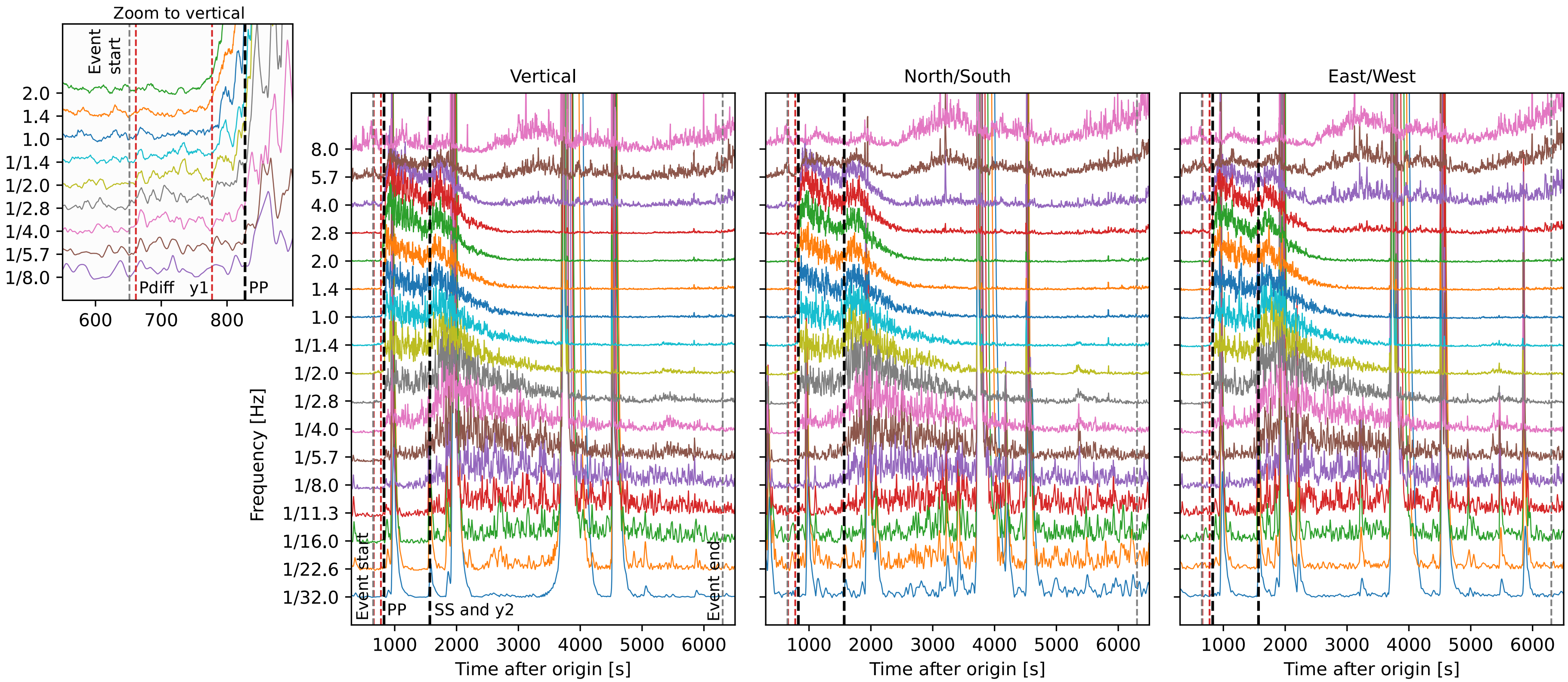

Figure S5: Filterbank for S1000a, computed using the 20 samples–per–second VBB (very broadband) data for vertical, north and east components. The inset zooms into the vertical component around the Pdiff and PP phase picks to show the onset of Pdiff. The dashed black lines show PP and SS identifications. The grey dashed lines mark the event start and end times. An additional phase identification labelled as y1 is shown with red dashed line before the PP phase. The y2 phase is coincident with the SS phase. The filterbanks are centered around the indicated frequencies, and half an octave wide on each side. The broad spectrum of the frequency content in this event is almost unique within the Marsquake catalogue.

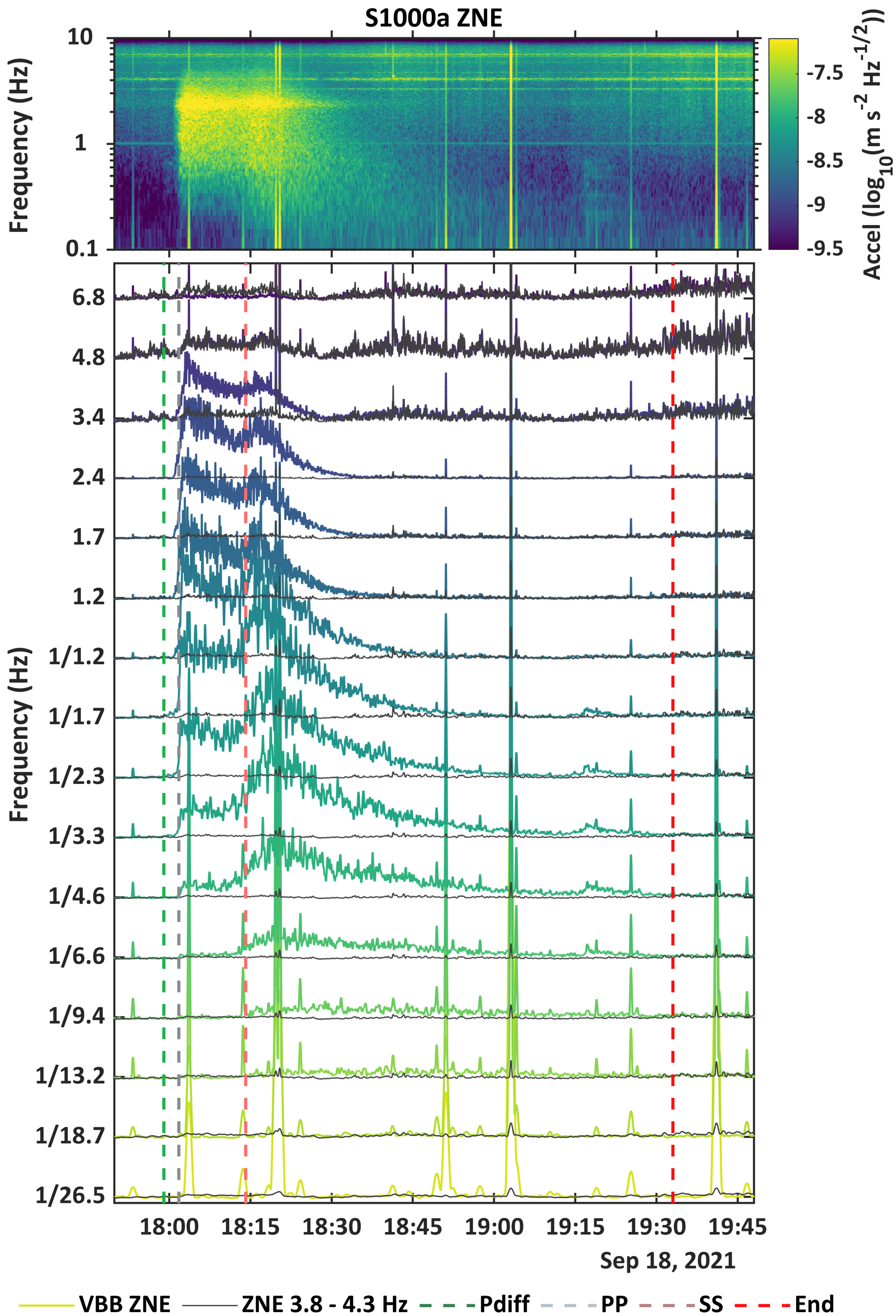

Figure S6: Comodulation for S1000a. Top panel: combined energy spectrogram for VBB (very broadband) ZNE 20sps data. Lower panel: VBB ZNE power envelopes and VBB ZNE power between 3.8 – 4.3 Hz in different frequency bands. The Pdiff, PP and SS phases are marked by the green, grey and orange vertical dashed lines respectively. Event end as catalogued by the MQS is marked by the vertical red dashed line. Note the clear divergence of the seismic power from the proxy for atmospheric power from 3.4 Hz to 1/13.2 Hz and that the SS phase extends down into lower frequencies than the PP phase. The secondary event, S1000b is evident between 19:15 and 19:30.

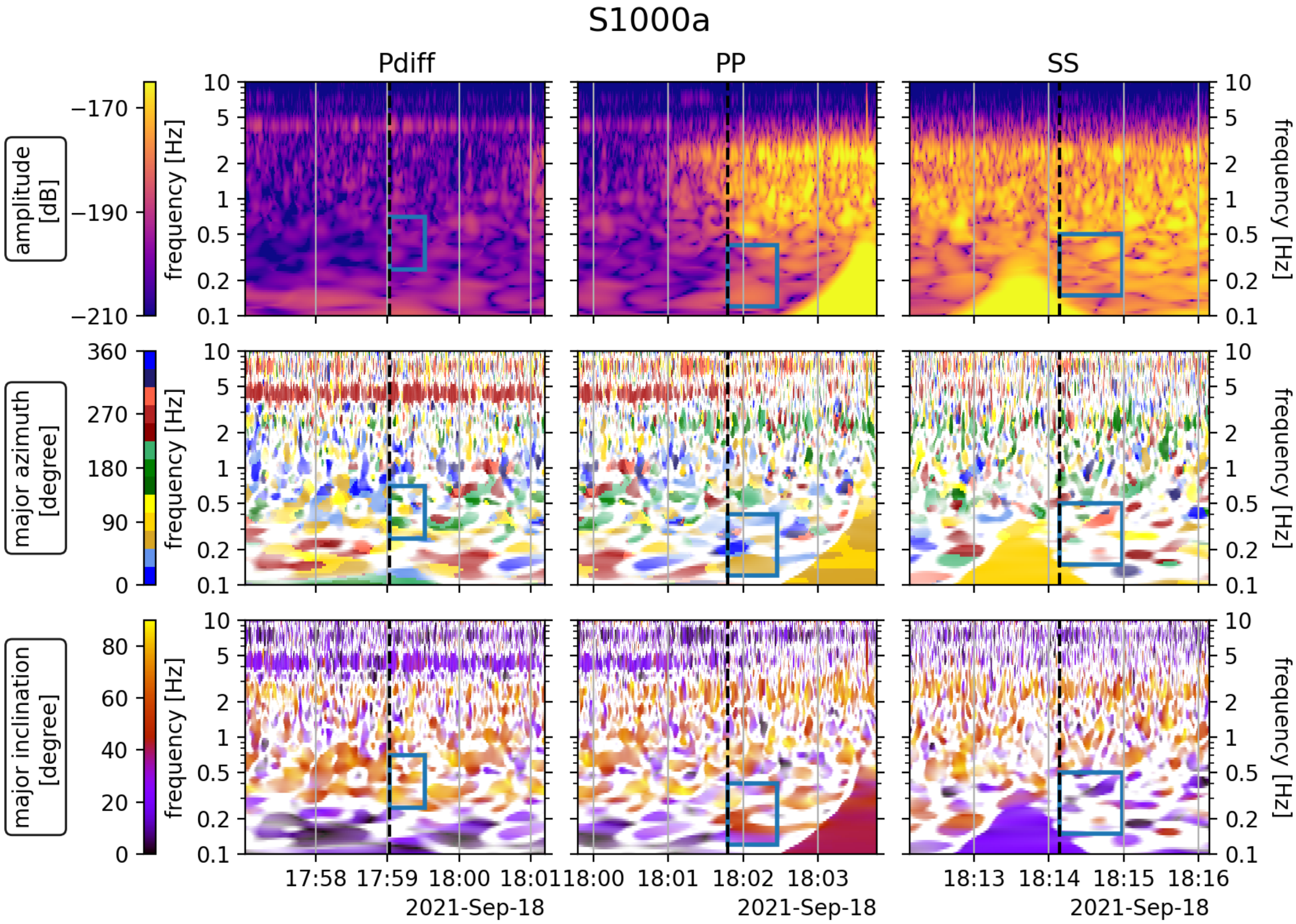

Figure S7: Polarisation analysis for marsquake S1000a. Shown are frequency-time plots of (top) signal amplitude in $(m/s)^2/Hz$ [dB], (middle) backazimuth, and (bottom) inclination. The time axis is zoomed in on the (left) Pdiff, (middle) PP, and (right) SS phase pick. Picks are marked with a vertical dashed line. Features to interpret are highlighted by blue boxes. Signals with weak polarisation are masked in the second and third row. Note the vertical major inclination angle at the onset of the Pdiff and PP phases and the horizontal inclination for SS. No clear backazimuth determination was possible for this event.

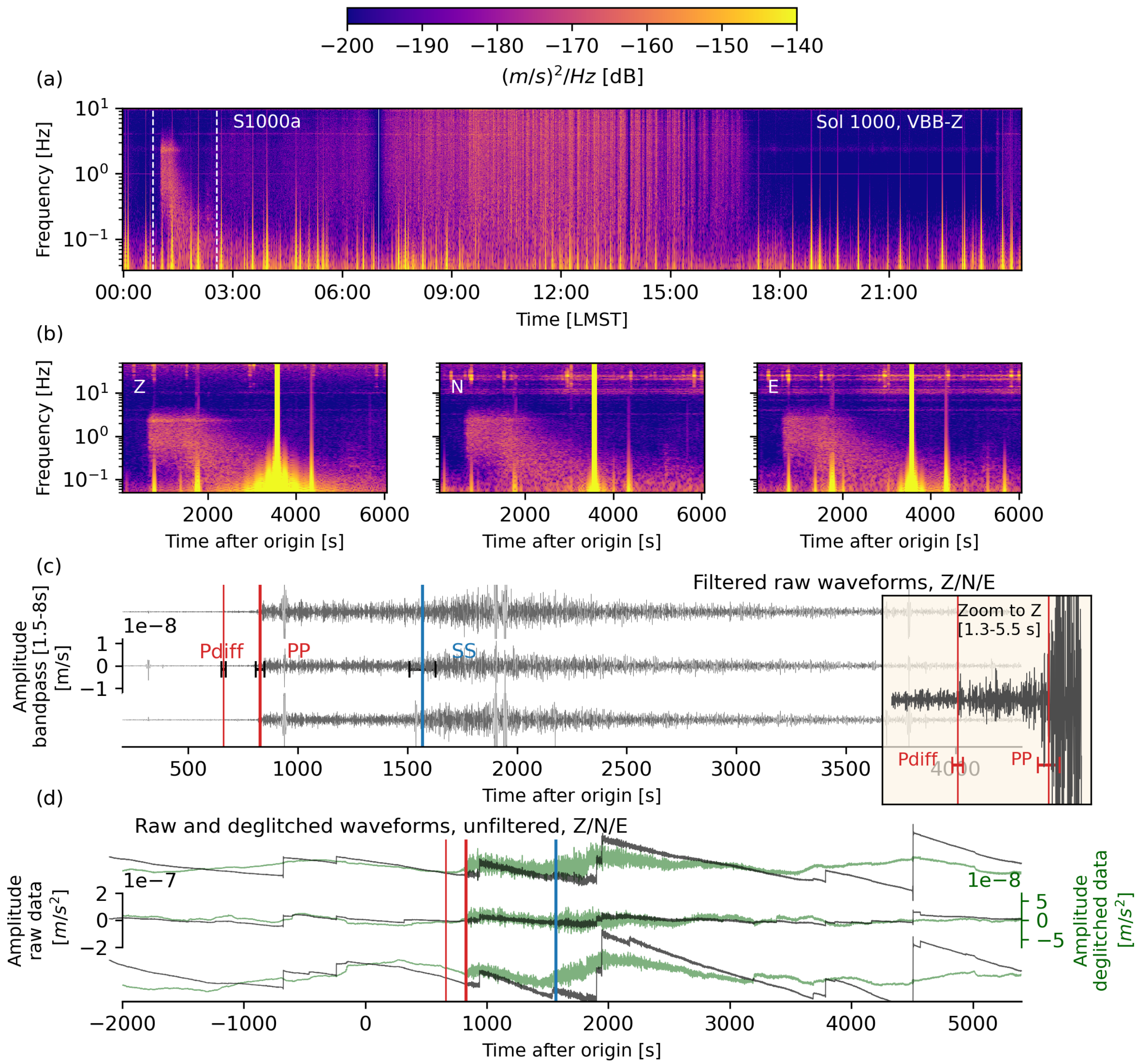

Figure S8: Overview of S1000a. (a) Sol-long velocity spectrogram (window length 120 s with 50% overlap) for 20 sps VBB (very broadband) vertical component. The event is marked with dashed vertical lines in the early hours from the origin time and signal end as identified by the MQS. (b) three-component velocity spectrograms for 100 sps VBB around the S1000a event (window length 120 s with 80% overlap), for the time period as marked in panel a. (c) Bandpass filtered (1.5–8 s) waveforms. The seismic phase picks of the MQS are shown with vertical lines as labelled. The horizontal error bars indicate the picking uncertainties. The inset plot zooms into the time frame around Pdiff and PP arrivals. (d) Unfiltered waveforms before (raw; black, left axis) and after deglitching (green, right axis) in acceleration. The same seismic phase picks on panel (c) are indicated as vertical lines with the same colours. The long-period drift including the glitches as steps in acceleration are clearly visible on the raw waveforms and are a common feature throughout the data from SEIS (Seismic Experiment for Interior Structure) but do not affect the picks when the data is filtered.

Table S3: Approximate onset time of glitches and donks during S1000a

Time (UTC)	Relative time (s)	Artefact type
2021-09-18 17:53:18	318	Glitch
2021-09-18 17:55:58	478	Donk
2021-09-18 18:01:14	794	Donk
2021-09-18 18:03:00	900	Donk
2021-09-18 18:03:28	928	Donk
2021-09-18 18:03:38	938	Glitch
2021-09-18 18:13:38	1538	Glitch
2021-09-18 18:15:55	1675	Donk
2021-09-18 18:18:23	1823	Glitch
2021-09-18 18:18:44	1844	Donk
2021-09-18 18:19:43	1903	Glitch
2021-09-18 18:20:25	1945	Glitch
2021-09-18 18:24:14	2174	Glitch
2021-09-18 18:37:56	2996	Donk
2021-09-18 18:39:36	3096	Donk
2021-09-18 18:39:57	3117	Donk
2021-09-18 18:41:20	3200	Donk;Glitch
2021-09-18 18:49:23	3683	Glitch
2021-09-18 18:51:05	3785	Glitch
2021-09-18 18:52:23	3863	Glitch
2021-09-18 19:00:39	4359	Donk
2021-09-18 19:03:07	4507	Glitch
2021-09-18 19:03:55	4555	Donk
2021-09-18 19:04:07	4567	Glitch
2021-09-18 19:18:54	5454	Glitch
2021-09-18 19:25:18	5838	Glitch

References

Ceylan, S., Clinton, J. F., Giardini, D., Böse, M., Charalambous, C., van Driel, M., Horleston, A., Kawamura, T., Khan, A., Orhand-Mainsant, G., Scholz, J.-R., Stähler, S. C., Euchner, F., Banerdt, W. B., Lognonné, P., Banfield, D., Beucler, E., Garcia, R. F., Kedar, S., Panning, M. P., Pike, W. T., Smrekar, S. E., Spiga, A., Dahmen, N. L., Hurst, K., Stott, A. E., Lorenz, R. D., Schimmel, M., Stutzmann, E., ten Pierick, J., Conejero, V., Pardo, C., and Perrin, C. (2021). Companion guide to the marsquake catalog from InSight, Sols 0–478: Data content and non-seismic events. *Phys. Earth Planet. In.*, 310:106597.

Charalambous, C., Stott, A. E., Pike, W. T., McClean, J. B., Warren, T., Spiga, A., Banfield, D., Garcia, R. F., Clinton, J., Stähler, S., Navarro, S., Lognonné, P., Scholz, J.-R., Kawamura, T., van Driel, M., Böse, M., Ceylan, S., Khan, A., Horleston, A., Orhand-Mainsant, G., Sotomayor, L. M., Murdoch, N., Giardini, D., and Banerdt, W. B. (2021). A comodulation analysis of atmospheric energy injection into the ground motion at InSight, Mars. *J. Geophys. Res.: Planets*, 126(4):e2020JE006538.

Clinton, J. F., Ceylan, S., van Driel, M., Giardini, D., Stähler, S. C., Böse, M., Charalambous, C., Dahmen, N. L., Horleston, A., Kawamura, T., Khan, A., Orhand-Mainsant, G., Scholz, J.-R., Euchner, F., Banerdt, W. B., Lognonné, P., Banfield, D., Beucler, E., Garcia, R. F., Kedar, S., Panning, M. P., Perrin, C., Pike, W. T., Smrekar, S. E., Spiga, A., and Stott, A. E. (2021). The Marsquake catalogue from InSight, sols 0–478. *Phys. Earth Planet. In.*, 310:106595.

Dahmen, N. L., Zenhäusern, G., Clinton, J. F., Giardini, D., Stähler, S. C., Ceylan, S., Charalambous, C., van Driel, M., Hurst, K. J., Kedar, S., Lognonné, P., Murdoch, N., Myhill, R., Panning, M. P., Pike, W. T., Schimmel, M., Schmelzbach, C., Scholz, J., Stott, A. E., Stutzmann, E., and Banerdt, W. B. (2021). Resonances and lander modes observed by InSight on Mars (1–9 Hz). *B. Seismol. Soc. Am.*, 111(6):2924–2950.

Kanamori, H. (1977). The energy release in great earthquakes. *J. Geophys. Res. (1896-1977)*, 82(20):2981–2987.

Kim, D., Davis, P., Lekić, V., Maguire, R., Compaire, N., Schimmel, M., Stutzmann, E., C. E. Irving, J., Lognonné, P., Scholz, J., Clinton, J., Zenhäusern, G., Dahmen, N., Deng, S., Levander, A., Panning, M. P., Garcia, R. F., Giardini, D., Hurst, K., Knapmeyer-Endrun, B., Nimmo, F., Pike, W. T., Pou, L., Schmerr, N., Stähler, S. C., Tauzin, B., Widmer-Schnidrig, R., and Banerdt, W. B. (2021). Potential pitfalls in the analysis and structural interpretation of seismic data from the Mars InSight mission. *B. Seismol. Soc. Am.*, 111(6):2982–3002.

Samson, J. C. (1983). The spectral matrix, eigenvalues, and principal components in the analysis of multichannel geophysical data. *Ann. Geophys.*, 1:115–119.

Samson, J. C. and Olson, J. V. (1980). Some comments on the descriptions of the polarization states of waves. *Geophys. J. Int.*, 61(1):115–129.

Schimmel, M. and Gallart, J. (2003). The use of instantaneous polarization attributes for seismic signal detection and image enhancement. *Geophys. J. Int.*, 155(2):653–668.

Schimmel, M., Stutzmann, E., Ardhuin, F., and Gallart, J. (2011). Polarized earth's ambient microseismic noise. *Geochem., Geophys., Geosyst.*, 12(7):Q07014.

Scholz, J.-R., Widmer-Schnidrig, R., Davis, P., Lognonné, P., Pinot, B., Garcia, R. F., Hurst, K., Pou, L., Nimmo, F., Barkaoui, S., de Raucourt, S., Knapmeyer-Endrun, B., Knapmeyer, M., Orhand-Mainsant, G., Compaire, N., Cuvier, A., Beucler, E., Bonnin, M., Joshi, R., Sainton, G., Stutzmann, E., Schimmel, M., Horleston, A., Böse, M., Ceylan, S., Clinton, J., van Driel, M., Kawamura, T., Khan, A., Stähler, S. C., Giardini, D., Charalambous, C., Stott, A. E., Pike, W. T., Christensen, U. R., and Banerdt, W. B. (2020). Detection, analysis, and removal of glitches from InSight's seismic data from Mars. *Earth Space Sci.*, 7(11):e2020EA001317.

Stutzmann, E., Schimmel, M., Lognonné, P., Horleston, A., Ceylan, S., van Driel, M., Stahler, S., Banerdt, B., Calvet, M., Charalambous, C., Clinton, J., Drilleau, M., Fayon, L., Garcia, R. F., Giardini, D., Hurst, K., Jacob, A., Kawamura, T., Kenda, B., Margerin, L., Murdoch, N., Panning, M., Pike, T., Scholz, J.-R., and Spiga, A. (2021). The polarization of ambient noise on mars. *J. Geophys. Res. Planets*, 126(1):e2020JE006545.